ACS Catalysis

Article

Trace Amount of SnO2-decorated ZnSn(OH)6 as Highly Efficient Photocatalyst for Decomposition of Gaseous Benzene: Synthesis, Photocatalytic Activity and the Unrevealed Synergistic Effect between ZnSn(OH)6 and SnO2

Xianliang Fu, Jinghui Wang, Danwei Huang, Sugang Meng,
Zizhong Zhang, Longfeng Li, Tifang Miao, and Shifu Chen

ACS Catal., **Just Accepted Manuscript** • DOI: 10.1021/acscatal.5b02593 • Publication Date (Web): 30 Dec 2015

Trace Amount of SnO_2-decorated $ZnSn(OH)_6$ as Highly Efficient Photocatalyst for Decomposition of Gaseous Benzene: Synthesis, Photocatalytic Activity and the Unrevealed Synergistic Effect between $ZnSn(OH)_6$ and SnO_2

Xianliang Fu[†*], Jinghui Wang[†], Danwei Huang[†], Sugang Meng[†], Zizhong Zhang[§], Longfeng Li[†], Tifang Miao[†], Shifu Chen[†‡*]

[†] College of Chemistry and Material Science, Huaibei Normal University, Huaibei, Anhui, China, 235000.

[‡] Department of Chemistry, Anhui Science and Technology University, Fengyang, Anhui, China, 233100.

[§] Research Institute of Photocatalysis, State Key Laboratory of Photocatalysis on Energy and Environment, Fuzhou University, Fuzhou, China, 350002.

ABSTRACT

It is still a challenge to develop a high performance photocatalyst for the abatement of aromatic compounds like benzene (C_6H_6) that has been regarded as a priority hazardous VOC substance in the indoor atmosphere. Zinc hydroxystannate ($ZnSn(OH)_6$, ZHS) is a promising material for the application. However, the key structural features which responsible for the high activity are still ambiguous. To address this issue, a series of ZHS with different surface properties was hydrothermally synthesized by varying the treatment temperature and the solution pH. Although ZHS can be readily synthesized under a mild reaction condition (Tem. 90-120 ^{o}C, pH 4-10), most of the samples were contaminated by trace amount of low-crystalized SnO_2. Pristine ZHS can only be produced in a strong alkaline solution (pH 13). The sample prepared at 120 ^{o}C in a pH 10 solution shows the highest activity for the degradation of gaseous C_6H_6 and the efficiency almost six times higher than P25 (TiO_2). More importantly, no obvious deactivation of the sample and the formation of stable deposits were observed in a long-term reaction for 48 h. Although SnO_2 amount is quite small and bare ZHS shows almost no activity, both of them are indispensable for the degradation of C_6H_6. SnO_2 and ZHS can be understood as photoactive sites to produce charge carriers and preferential sites for the adsorption of O_2, H_2O, and C_6H_6, respectively. A synergistic effect between SnO_2 and ZHS in the formation of active radicals and the degradation of C_6H_6 accounts for the high performance of the SnO_2 decorated ZHS.

KEYWORDS: zinc hydroxystannate, tin dioxide, photocatalysis, benzene degradation, synergistic effect, photoactive sites

1. INTRODUCTION

As an important solvent and raw material, benzene (C_6H_6) is widely used in industry for producing drugs, dyes, insecticides, and plastics. It is a widespread volatile organic compound

(VOC) in the polluted indoor atmosphere. Due to its high carcinogenicity and environmental persistence,[1] C_6H_6 has been regarded as a priority hazardous substance.[2] Developing a highly efficient treatment technology for the abatement of highly stable C_6H_6 remains an unanswered challenge at ambient condition.

Presently, the methods for the elimination of VOCs are mainly focused on active carbon adsorption, catalytic combustion, and photocatalytic oxidation (PCO).[3] Among them, TiO_2 based PCO is a promising technology for the treatment of low concentration of VOCs in ppb-ppm level. Compared to a physical adsorption process, the mineralization of VOCs can be achieved by PCO only through the use of air and light at room temperature. The operating condition is much milder than the catalytic combustion process which is generally performed at a high temperature (ca. 300 ^{o}C).[3c] Although numerous VOCs can be readily removed by PCO, unfortunately, limited success has been achieved in the treatment of aromatic compounds like benzene and toluene. Due to the deposition of tar or stable carbonaceous by-products,[4] the oxidation reactions cannot be sustained for a long time on some typical photocatalysts such as TiO_2 and ZnO.[4a, c, d, 5] To deal with the issue of low efficiency, several approaches have been explored to improve the decomposition efficiency of C_6H_6, including modifying a photocatalyst with noble metals (Pt, Pd, or Rh),[6] introducing H_2O vapor or H_2 into the reaction system,[7] and developing new highly efficient photocatalyst instead of the inefficient TiO_2.[4d, 8] The third approach is clearly more attractive than the former two in consideration of the high cost of the noble metals and the complexity of the hybrid system.

In theory, PCO can be promoted by a hydroxyl material as the fact that photocatalytical degradations are mainly triggered by hydroxyl radical (·OH) whose formation was favored by a surface with a high population of OH.[9] In addition, PCO can also be induced directly by photo-

generated hole (h^+). Both the routes can lead to the decomposition of the most pollutants.[10] However, as for the decomposition of benzene, ·OH mediated degradation route is more crucial than the latter because the reported works[11] indicated that a free radical polymerization would be induced by the attack of C_6H_6 with h^+, which resulted in the deposition of stable coke. The beneficial effect of hydroxyl structure for PCO abatement of C_6H_6 is also supported by reported hydroxide photocatalysts, such as $In(OH)_3$, $ZnSn(OH)_6$, InOOH, GaOOH, $CaSn(OH)_6$, $SrSn(OH)_6$.[4a, 12] Among them, the low cost Sn-based hydroxides are more realistic for practical application due to the rarity and high cost of In and Ga. $ZnSn(OH)_6$ (ZHS) is a perovskite-structured hydroxide. We first found that the degradation of gaseous C_6H_6[4a] and the reforming of ethanol to H_2 and CH_4[13] can be achieved on ZHS via a photocatalytic process. Its versatility was further confirmed by PCO of methyl orange (MO), cyclohexane, phenol and nitrogen monoxide.[14] However, some inconsistent results were also observed recently.[15] These works indicated that not all the prepared ZHS samples showed high activity for the degradation of C_6H_6. The light absorption, morphology, and activity of ZHS highly depend on the preparation route. Then a question arises, which structural features are essentially responsible for PCO activity of ZHS and how the preparation condition affects them? A comprehensive investigation of these issues will not only benefit the understanding of PCO mechanism of ZHS, but also contribute to the development of high performance photocatalyst based on hydroxides for benzene abatement.

Herein, a series of ZHS with different surface properties was hydrothermally synthesized. The effects of the preparation condition including the hydrothermal temperature and the solution pH on the formation and the properties of ZHS were investigated systematically. The aim of this work is to reveal the key structural features of ZHS, which favour the degradation of C_6H_6. The

results indicated that the high performance ZHS samples were contaminated by trace amount of low-crystalized SnO_2. A synergistic effect between SnO_2 and ZHS in the formation of active radicals and the degradation of C_6H_6 accounts for the high performance of SnO_2 contaminated ZHS. Both of them are indispensable for the degradation of C_6H_6.

2. EXPERIMENTAL SECTION

2.1 Chemicals and Preparation of ZSH.

Analytically pure $Na_2SnO_3{\cdot}4H_2O$, $ZnCl_2$, NaOH, hydrochloric acid (37%), and MO were purchased from Sinopharm Chemical Reagent Co. Ltd and used as received. The spin-trap reagent 5, 5-dimethyl-1-pyrroline-N-oxide (DMPO) was purchased from Sigma Chemical Co.

ZHS samples were prepared by a hydrothermal method. In a typical procedure, 20 mL 2 mM $ZnCl_2$ solution was first introduced into a 50 mL PTFE vessel. 20 mL 2 mM Na_2SnO_3 solution was added drop wise to the solution under vigorous stirring. After the addition, the pH of the white suspension was adjusted to a desired value (1-13) by 0.15 M HCl or NaOH solution. The resulted suspension was then transferred into an autoclave and heated at a desired temperature (20-180 ^{o}C) for 24 h. The product formed after the treatment was carefully recovered by centrifugation, rinsing thoroughly with deionized water, and finally dried at 95 ^{o}C for 4 h. The effects of the solution pH (with temperature fixed at 120 ^{o}C) and the hydrothermal temperature (with solution pH fixed at 10) on the formation of ZHS were investigated, respectively.

For comparison, pristine SnO_2 and ZnO were prepared via a similar hydrothermal route by using only one of the precursors in a neutral solution. The solution pH was adjusted by 0.15 M HCl or NaOH solution.

2.2 Characterization

X-ray diffraction (XRD) patterns were performed on a Bruker D8 Advance diffractometer by using Ni filtered Cu Kα radiation λ = 1.5406 Å. The UV–Vis optical absorption spectra (UV-vis DRS) were recorded on a Shimadzu UV 3600 UV–Vis–NIR spectrometer with $BaSO_4$ as a reference. The morphologies were examined by using a field emission scanning electron microscopy (SEM, SU8000, Hitachi) and a transmission electron microscopy (TEM, FEI Tecnai G2 F20 S-TWIN). N_2 adsorption–desorption isotherms were obtained at 77 K by using a Micromeritics Tristar II 3020 surface area analyzer. Multipoint Brunauer-Emmett-Teller (BET) specific surface areas were then determined from the linear part of the BET transform of the adsorption isotherms. Fourier transform infrared (FTIR) spectra were recorded on a Thermo Nicolet Nexus 6700 FTIR spectrophotometer by using KBr pellets.

2.3 Photocatalytic Measurements

Both liquid-solid and gas-solid photocatalytic activities of the prepared samples were evaluated by using MO solution and gaseous C_6H_6 as a model of pollutant, respectively. The schematic diagram of the reaction systems had been described in our former works[15b] and their pictures are shown in Figure S1 (Supporting information). The degradation of MO reactions was carried out in a 200 mL tubular reactor which surrounded by a water cooling jacket. A 9 W H-shaped low pressure mercury UV lamp (254 nm, Philips TUV PLS-9w) was assembled at the center of the reactor. In a typical experiment, 100 mg ZHS was dispersed in 200 mL 10 ppm MO aqueous solution and then magnetically stirred for 30 min in the dark to reach an adsorption-desorption equilibrium. The solution was ventilated with air (20 mL/min) throughout the reaction and its temperature was controlled at 20 ^{o}C by circulating water. During irradiation, a 3 mL solution was withdrawn through a pipette every 20 min followed by a centrifugation at 10000 rpm for 3 min. The concentration of the residual MO in the supernatant was monitored by a spectrophotometer

(Shimadzu UV 3600 UV–Vis–NIR Spectrometer). The experimental error was estimated within 5% by repeating runs.

Photocatalytic degradation of gaseous C_6H_6 was performed in a fixed-bed tubular mico-reactor with a continuous flow mode. The reactor is made of a quartz tube with a length of 250 mm and an inner diameter of 4 mm, which was surrounded by four 6 W UV lamps (254 nm, TUV 6W/G6 T5, Philips). The heat generated by the lamps was removed by a suction fan and the reactor temperature was controlled at ca. 30 ^{o}C. In a typical experiment, 0.1 g ZHS was first mixed thoroughly with 1.0 g 50-70 mesh high purity quartz sands (as support material). The mixture was then loaded into the reactor. Benzene vapor was supplied by a gas cylinder at a constant concentration of 250 ppm with the balance of O_2 (Dalian Da'te ga Co., Ltd.). The flow velocity was kept at 30 mL/min corresponding to a reactor residence time of 1.8 s. Simultaneous determination of C_6H_6 and the formed CO_2 were performed on an online gas chromatograph (Agilent 7820A) with a FID and a TCD detector, respectively. The conversion (CE, C%) and the mineralization efficiency (ME, M%) of C_6H_6 were calculated according to the steady-state reaction data by Eq. 1 and Eq. 2, respectively. The degradation (r_d, $\mu mol \cdot g^{-1} \cdot h^{-1}$) and mineralization ($r_m$, $\mu mol \cdot g^{-1} \cdot h^{-1}$) rates of C_6H_6 on the samples were calculated by Eq. 3 and Eq. 4, respectively. The feed gas was treated as ideal gas for the calculations.

$$C\% = \frac{[C_6H_6]_{initial} - [C_6H_6]_{steady}}{[C_6H_6]_{initial}} \quad \text{(Eq. 1)}$$

$$M\% = \frac{[CO_2]_{steady}}{([C_6H_6]_{initial} - [C_6H_6]_{steady}) \times 6} \quad \text{(Eq. 2)}$$

$$r_D = \frac{[C_6H_6]_{initial} \times 30(mL/min) \times 60(min) \times C\%}{22.4(L/mol) \times 0.1(g)} \quad \text{(Eq. 3)}$$

$r_M = r_D \times M\%$ (Eq. 4)

2.4 Active Radicals Measurement

The formation of the active radicals in the suspension of selected sample was measured by electron spin resonance (ESR) technique with the use of DMPO as a spin-trap agent. The ESR signals of the trapped radicals were recorded at ambient temperature on a Brucker ESR 300 E spectrometer. All freshly-prepared suspensions (for ·OH measurement: DMPO: 0.20 M, 20 μL + 0.5 mL water; for $O_2^{\cdot -}$ measurement: DMPO: 0.20 M, 20 μL + 0.5 mL methanol; sample: 10 mg) were mixed directly and then transferred into a cylindrical quartz cell (length 100 mm, diameter 2 mm). A spot UV-light source (Hamamatsu LC8, equipped with a narrow-band-pass filter of 254 nm) was used in situ as a light source. The signals were taken every 40 s.

3. RESULTS AND DISCUSSION

3.1 Effects of Preparation Conditions on ZSH Formation

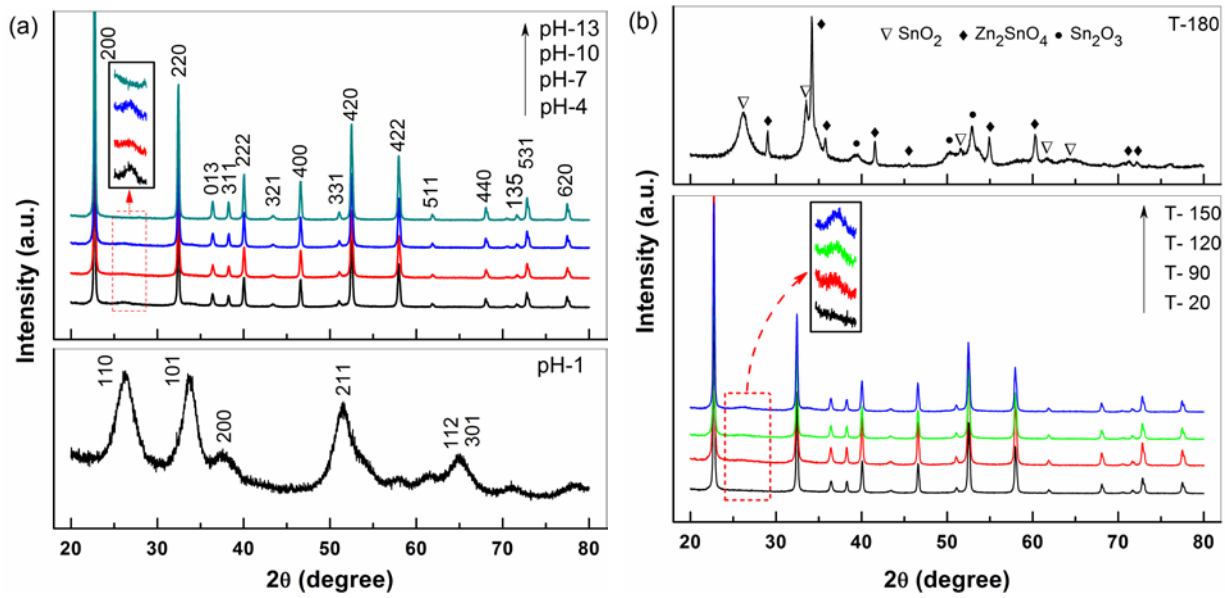

Figure 1 XRD patterns of the products prepared at (a) different solution pH and (b) different temperature.

Figure 1a and 1b shows the XRD patterns of the samples prepared at different solution pH and different hydrothermal temperature, respectively. As shown in Figure 1a, the sample prepared at pH 1 shows some weak and broad diffraction peaks which can be indexed to the tetragonal SnO_2 (JCPDS No. 77-449). The hydrolysis of $[SnO_3]^{2-}$ in the acidic solution[16] accounts for the formation of SnO_2, while Zn precursor is still in Zn^{2+} state at pH 1. No any ZHS peak can be found in the pattern. However, when the solution pH was increased to 4, a well-crystallized ZHS sample was formed via Eq. 5 due to the hydrolyzation of Na_2SnO_3 to $[Sn(OH)_6]^{2-}$.[17] The pattern can be ascribed to the cubic phase of $ZnSn(OH)_6$ (JCPDS No. 073-2384). However, a small broad peak located at $2\Theta=26^{o}$ is still present (as shown in the enlarged figure in Figure 1a). This peak can be assigned to the (110) reflection of the tetragonal SnO_2 as pure phase tetragonal SnO_2 has been formed at pH 1. Although the intermediated oxidation states tin oxides (i.e. Sn_2O_3, and Sn_3O_4) have a similar diffraction peak around $2\Theta=26^{o}$, these oxides are commonly formed during the conversion of SnO to SnO_2[18] or a heat treatment of SnO_2 at elevated temperature in the absence of excess oxygen[19] (formed by etching of lattice O atoms from SnO_2[20]). Here, as $SnCl_4$ was used as Sn precursor and the hydrothermal temperature is not too high (no higher than 160 ^{o}C), the formation of these intermediated oxidation samples are minimal. With further increasing the solution pH from 4 to 13, the intensity of ZHS peaks is slightly improved. Meanwhile, the inconspicuous SnO_2 peak fades away and is hard to be distinguished at pH 13. Obviously, the solution with a high pH value favors the formation of ZHS. As shown in Figure 1b, well-crystallized ZHS can be readily synthesized in a temperature range of 20-150 ^{o}C without adjusting the solution pH (at ca. 10). The (110) peak of SnO_2 is gradually promoted by increasing the temperature. It suggests that part of Sn precursor did not involve in the formation of ZHS at elevated temperature. With further increasing the temperature

to 180 °C, ZHS cannot sustain anymore and decomposes to the tetragonal SnO_2 and cubic Zn_2SnO_4 (JCPDS 74-2184) via Eq. 6. Small amount of triclinic Sn_2O_3 (JCPDS 25-1259) can also be observed in the product, which is formed by the etching of SnO_2 lattice oxygen atoms at high hydrothermal temperature.[20] The XRD results suggest that most of the well-crystallized ZHS samples are contaminated by some low-crystalized SnO_2 (denoted as S-ZHS hereafter). Low hydrothermal solution pH or high preparation temperature promotes the segregation of SnO_2 component. Although no ZnO diffraction peaks can be found in all the samples, ZnO may exist in an amorphous state. The possibility will be determined by UV-vis DRS analysis.

$$Zn^{2+} + [Sn(OH)_6]^{2-} \rightarrow ZnSn(OH)_6 \qquad \text{(Eq. 5)}$$

$$ZnSn(OH)_6 \rightarrow Zn_2SnO_4 + SnO_2 + 3H_2O \qquad \text{(Eq. 6)}$$

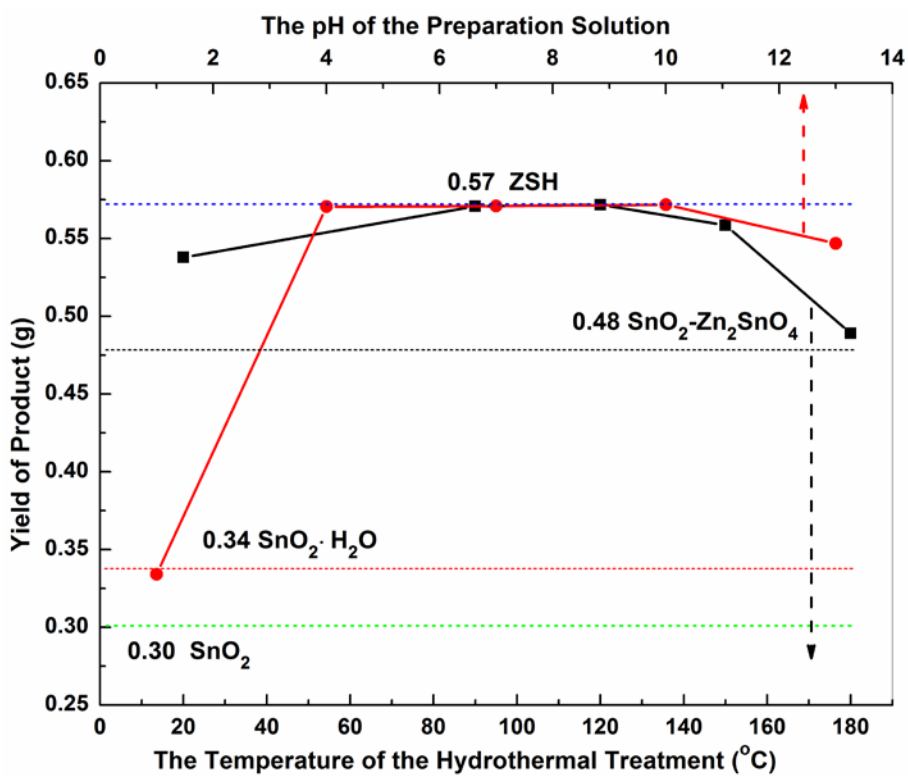

Figure 2 Yields of the product prepared at different solution pH and different hydrothermal temperature.

Although the phase composition and the structure of the prepared ZHS samples are tentatively investigated by XRD, Sn^{4+} and Zn^{2+} may be in form of amorphous oxides or hydroxides states which are hard to be disclosed by XRD technology, especially under the strong shielding effect of highly crystalized $ZnSn(OH)_6$. However, if the prepared samples were contaminated by these components, the yields of the products would be quite different. To assist the XRD analysis, the yields of the products under different preparation conditions were carefully determined. The XRD result (Figure 1) suggests that the products may be in form of SnO_2, ZHS, or SnO_2-Zn_2SnO_4. Thus, the corresponding theoretical yields are calculated to be 0.30, 0.57, and 0.48 g, respectively. As shown in Figure 2, the sample obtained at pH 1 is 0.33 g. It is slightly higher than the theoretical yield of SnO_2 suggesting the product may contain crystal water (in the form of $SnO_2 \cdot H_2O$[21]). The formation of ZHS can be largely achieved in the pH range of 4-10 as the yields are almost identical to the theoretical value. A slight drop of the yield is observed with further increasing the pH to 13. Unrevealed by the XRD result, the finding suggests that a surface etching process is occurred over ZHS in the strong basic solution for the amphoteric nature of Sn^{4+}.[22] The corrosion results in the disappearance of SnO_2 (110) peak in Figure 1a. These results suggest that the amount of SnO_2 (observed in the XRD patterns) is quite small and should present on ZHS surface rather than in its bulk. As for the effect of the hydrothermal temperature, a complete formation of ZHS cannot be achieved at room temperature and a treatment at 90-120 ^{o}C is required. Because of the thermal instability of ZHS, a slight decline in the yield can be observed when the temperature is beyond 120 ^{o}C. The yield (0.49 g) achieved at 180 ^{o}C is comparable to the theoretical value of SnO_2-Zn_2SnO_4 composite indicating a thorough breakdown of ZHS is occurred. Thus, the condition for high yield of ZHS is conducting the hydrothermal treatment in a solution with pH 4-10 at a mild temperature (90-120 ^{o}C).

3.2 UV-Vis DRS Analysis

UV-Vis DRS has been extensively used to study the electronic state information of a photocatalyst, as well as the information of the surface metal ions, such as the coordination symmetry and the valence state.[23] This technology was used to investigate the absorptions of the prepared samples and to further study their surface structures. The UV-Vis DRS of the prepared ZHS are shown in Figure 3. Consistent with our former works,[13, 15b] two absorption bands can be distinguished in the spectra. Taken the sample pH-4 (Figure 3a) as example, the spectrum can be deconvoluted into two bands: one is threshold at ca. 250 nm (B-250), and the other is at ca. 350 nm (B-350). Highly similar spectra have been observed in some Sn-containing samples, such as Sn-Zn layered double hydroxides and Sn-SBA-15.[24] The absorptions have been assigned to the charge-transfer transition from O^{2-} to Sn^{4+} which located in a different coordination environment. The absorptions are quite sensitive to the coordination structure of Sn^{4+}. Generally, the intrinsic absorption of hydroxides occurs in a deep UV region, such as $In(OH)_3$ and GaOOH.[12d, 25] Thus, B-250 can be ascribed to the intrinsic band transition of pristine ZHS. This absorption is hardly impacted by the preparation condition. As most of the ZHS samples are contaminated by low-crystallized SnO_2, B-350 can be ascribed to the absorption of SnO_2. Unlike B-250, the absorption decreases with the solution pH and vanishes at pH 13 (Figure 3a) due to the etching of SnO_2, but increases with the treatment temperature (Figure 3b). Apparently, the absorption band of B-350 and the SnO_2 (110) peak (Figure 1) share a same variation tendency with the change of the hydrothermal temperature or solution pH, suggesting the attribution of B-350 to SnO_2 is fairly reasonable.

Tauc plot approach[26] was used to determine the band gap energy (E_g) of the prepared ZHS samples:

$$K(h\nu-E_g)^{1/n} = F(R)h\nu$$

where F(R) is the absorption coefficient, hv is photon energy, K is a constant, and n equals 2 for direct transition of SnO_2[27]and ZHS[25b]. The plots are shown in the inset of Figure 3. Obviously, two E_g edges located at 3.5 and 5.0 eV can be observed for most of the samples except the one prepared at pH 13 (denoted as ZHS-13), which shows only the E_g of 5.0 eV. The absorption edge energies at 3.5 and 5.0 eV can be ascribed to the band gap transition of SnO_2[19a, 21a] and $ZnSn(OH)_6$[25b], respectively.

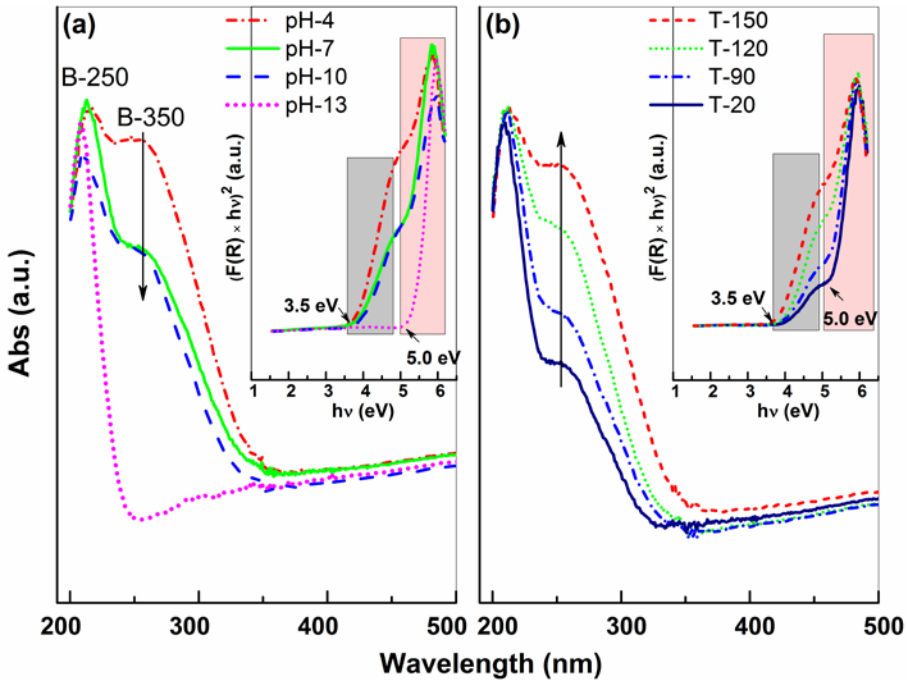

Figure 3 UV-Vis DRS of the samples prepared at (a) different pH solution and (b) different temperature. The insets show the Tauc plots.

For comparison, pristine SnO_2 and ZnO were prepared in a similar route by using only one of the precursors and the light absorptions of the samples were then characterized. The XRD results (Figure S2) indicated that a hexagonal ZnO (JCPDS No. 75-1526) and a tetragonal SnO_2 (JCPDS No. 77-449) samples were successfully synthesized. Figure S3 shows the UV-Vis DRS of the two samples. The onsets of the absorptions are at ca. 350 and 390 nm for SnO_2 and ZnO,

respectively. The result further confirms that B-350 originates from the band-gap absorption of SnO_2. As the prepared ZHS samples show no absorption around 390 nm and no ZnO diffraction peak is observed in Figure 1, the existence of ZnO on the prepared ZHS samples thus can be excluded. These results also rule out the presence of the heterovalent tin oxides as their E_g values are lower than 2.7 eV.[18b, 19a, 28]

3.3 Morphology

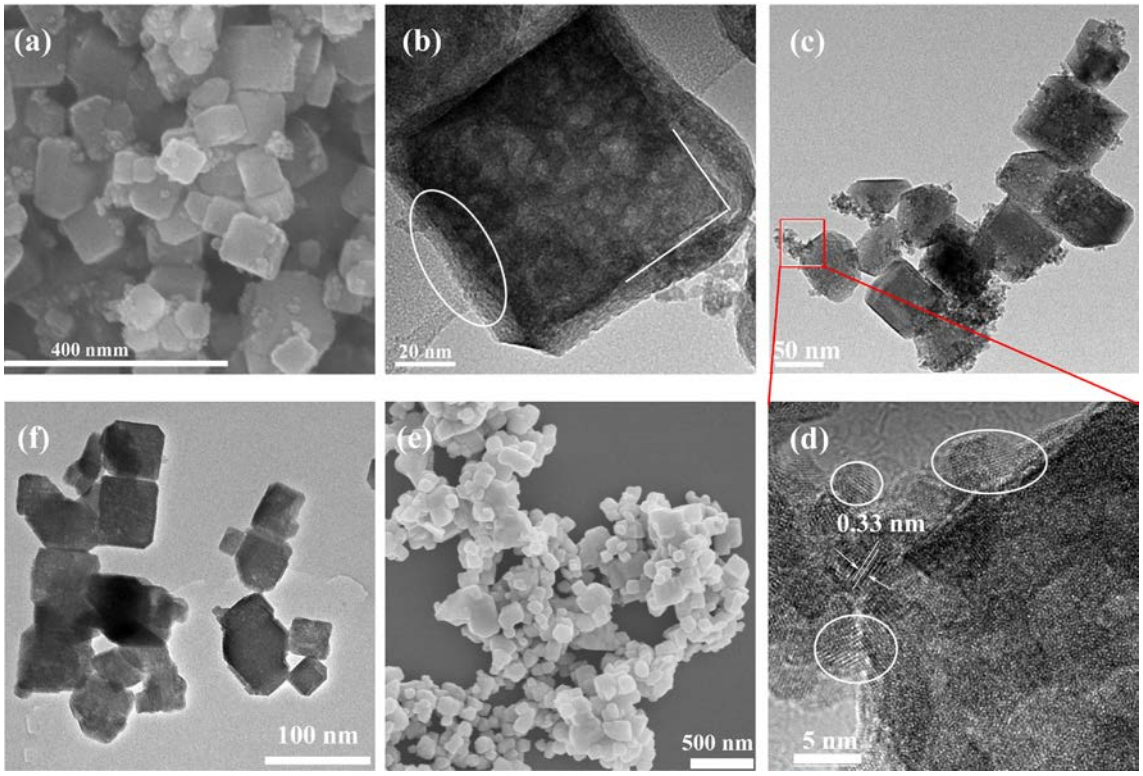

Figure 4 (a) SEM, and (b-d) TEM images of the ZHS prepared at pH 10 and (e) SEM, and (f) TEM images of the ZHS prepared at pH 13

The representative morphologies of the ZHS prepared at pH 10 (denoted as ZHS-10) and 13 (i.e. ZHS-13) were investigated by SEM and TEM. As the intrinsic structure of ZHS has a cubic symmetry, the samples are mainly composed of cubic particles (Figure 4). As shown in Figure 4a, the edge length of the cubes in ZHS-10 is in the range of 50 to 100 nm. The surface is coarse and some small nanoparticles contact tightly on the cubes. This morphology feature is further

confirmed by the TEM image (Figure 4b and c). HRTEM image (Figure 4d) indicates that the size of the nanoparticles is no more than 5 nm (as indicated by the cycles). A set of lattice fringes with the inter-plane spacing ca. 0.33 nm is present in the nanoparticles, which correspond to the d value of (110) plane of tetragonal SnO_2. As a type of hydroxides, the radiation damage of ZHS under the exposure of high energy of electron beam can be observed in Figure 4b. A layer of amorphous phase with a thickness about 4 nm is formed during the TEM observation. The angle between the two adjacent facets is ca. 90° suggesting the cube surface is dominated by six equivalent {100} facets.[29] As for the sample ZHS-13, the size of the cubes is comparable to that in the ZHS-10 sample (Figure 4e and f). However, the morphology becomes less uniform and the surface is even and compact. No any SnO_2 nanoparticles can be observed, consisting well with the XRD and UV-Vis DRS results. The smoothness of the surface and the absence of SnO_2 component imply that an etching process is occurred on sample ZHS-13 during the hydrothermal treatment. A similar phenomenon has been reported.[15a, 30]

3.4 Photocatalytic Activities

3.4.1 Decoloration of MO Solution

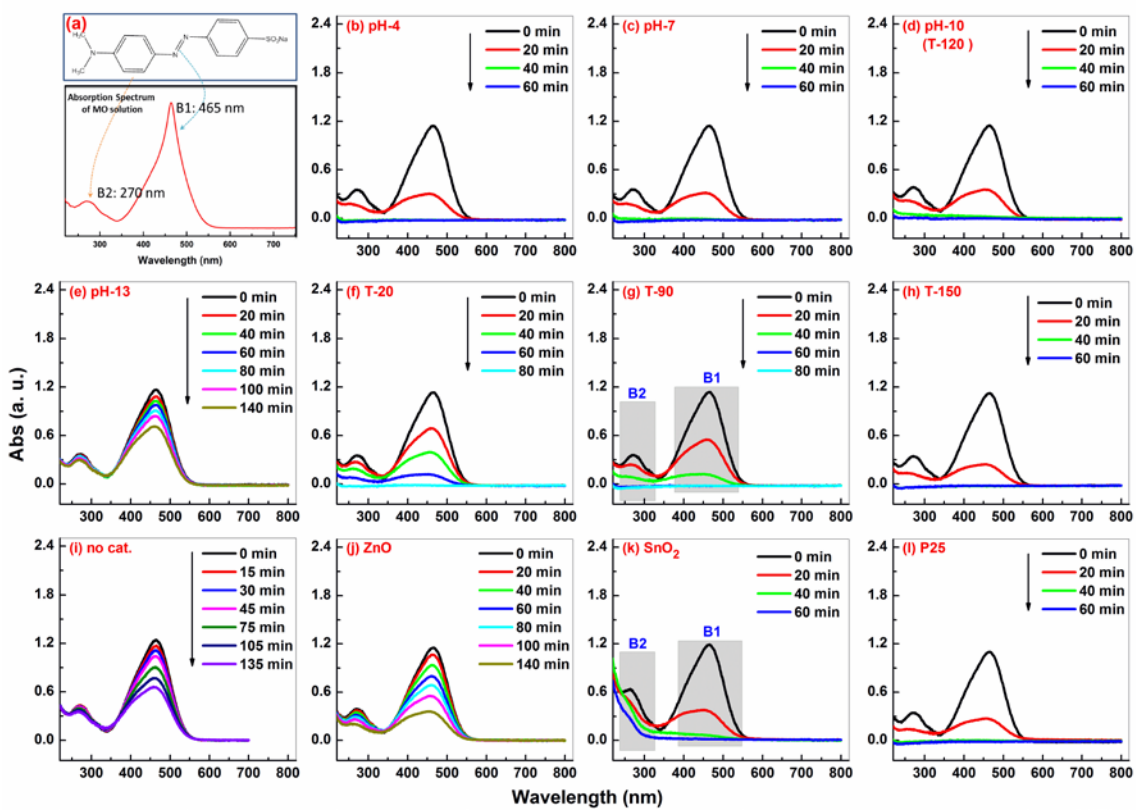

Figure 5 (a) Chemical structure of MO and its UV-Vis absorption spectrum and time-dependent absorption spectrum of MO on different samples under irradiation: (b-e) ZHS prepared at different pH, and (f-h) at different temperature, (i) no catalyst, (j) ZnO, (k) SnO_2 and (l) P25.

MO was chosen as a model of pollutant to investigate the liquid-solid degradation activity of the prepared ZHS samples. Using MO as the model has both practical and theoretical significances. It is a well-known dye pollutant in effluent from textile and other industrial processes.[31] On the other hand, as shown in Figure 5a, MO has an azo bond (N=N) which associates with chromophores (benzene rings, BRs) and auxochromes. The azo bond accounts for the maximum light absorption at 465 nm (B1), while the two BRs lead to the small absorption at 270 nm (B2).[32] Monitoring the variation of these bands, especially the B2, can disclose whether the sample has a capability to open the highly stable BR. Figure 5b-h shows the

time dependent photocatalytic decoloration of MO over the prepared ZHS samples. A significant degradation of MO can be observed on most of the ZHS samples (i.e. S-ZHS) except ZHS-13 and the MO solutions become colorless within ca. 40 min. The activities are comparable to the famous P25 (Figure 5l). More importantly, the BR can be successfully destroyed over these samples. A simultaneous decrease of B1 and B2 with illumination time can be observed. However, ZHS-13 (Figure 5e) shows no apparent activity. The decoloration of MO is slightly larger than a photolysis process (Figure 5i) and B2 also shows no significant change with irradiation time. Due to the use of high energy UV-C (254 nm), the breakage of the azo bond (B1) can be observed in the photolysis process. Similar decoloration process has been observed under irradiation.[15b, 32] However, B2 is not affected by the irradiation suggesting the BR cannot be cracked by UV-C. The activities of the as prepared ZnO and SnO_2 were also investigated and the results are shown in Figure 5j and k. Apparently, ZnO shows much lower activity than the prepared S-ZHS samples, while the activity of SnO_2 is comparative. However, the capability of SnO_2 to open the BR is substantially lower than that of S-ZHS samples (indicated by the rectangles in Figure **5**g and k). After irradiation for 40 min, although the solution is already colorless in SnO_2 suspension, the absorption band of B2 still can be found. It suggests that SnO_2 is more effective for cracking of the azo bond rather than the BR.

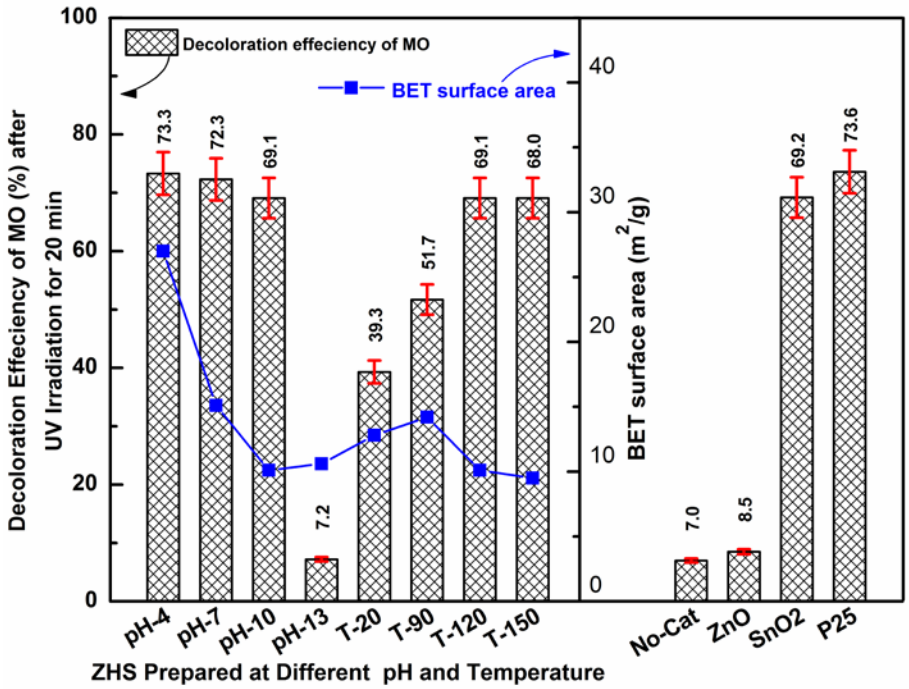

Figure 6 Decoloration efficiency of MO after irradiation for 20 min over the prepared ZHS samples and the compared photocatalysts.

To compare the photocatalytic performance of the ZHS samples, the decoloration efficiencies of MO after irradiation for 20 min are summarized in Figure 6 based on the variation of B1. It indicates that increasing the preparation solution pH from 4 to 10 brings a slight decrease of the decoloration efficiency, from 73.3% to 69.1%. With further increasing the pH to 13, the efficiency of the resulted sample (ZHS-13) drops sharply to only 7.2%. It is almost identical to the efficiency of the photolysis process (7.0%). As for the effect of the preparation temperature, the efficiency is improved considerably with the temperature, from 39.3% (20 ^{o}C) to 69.1% (120 ^{o}C), and then remains almost constant. The samples prepared at low pH (4-7) or at mild temperature (120-150 ^{o}C) show no remarkable difference for the degradation of MO. On these samples, the cleavage of the azo bond efficiency is comparable to that of SnO_2 (69.2%) and famous P25 (73.6%), but much larger than that of ZnO (only 8.5%).

The N_2 adsorption–desorption isotherms of the prepared ZHS were determined at 77 K (Figure S4) and the BET surface areas were then calculated from the BET transform plot of $1/Q[(P_0/P)-1]$ versus P/P_0 (the insert of Figure S4). The samples have IV-type isotherms with a small hysteretic loop according to the IUPAC classification. For the samples prepared at different pH, the areas decrease in the order 27.0 (pH 4) > 15.1 (7) > 10.1 (10) ≈ 10.6 m^2/g (13). For the samples prepared at different temperature, the area increases slightly from 12.8 to 14.2 m^2/g with temperature from 20 ºC to 90 ºC, and then reduces from 10.1 (120 ºC) to 9.5 m^2/g (150 ºC). An association analysis has been made to disclose the relationship between the activity of ZHS and its surface area. As shown in Figure 6, there is no consistent relationship between them suggesting the different activity should be mainly controlled by other factors rather than only the surface area. It is more likely to be the presence of SnO_2 considering the degradation efficiency exhibits almost the same varying trend as that of the SnO_2 amount (estimated by the SnO_2 (110) peak intensity shown in Figure 1) with change of the preparation conditions. The assumption is also supported by the fact that, after removing SnO_2 component, no obvious photocatalytic activity was observed on the sample ZHS-13.

3.4.2 Decomposition of Gaseous Benzene

The degradation of MO indicates that S-ZHS samples have a great capability to cleave the BR, as well as P25. However, the decomposition and the mineralization of benzene in the gas atmosphere may be quite different to that in a liquid medium for the deficiency of water which is crucial for the elimination of VOCs.[11a, 33] To verify the validity of S-ZHS and to study the effects of the preparation conditions on the activity, PCO of gaseous C_6H_6 was further evaluated in a plug flow mico-reactor with a continuous flow mode. As shown in Figure S5-A and B, excluding ZHS-13 (Figure S5-A-d), the degradation of C_6H_6 can be achieved on the prepared ZHS samples

(i.e. S-ZHS samples). C_6H_6 concentration drops immediately after turning on the UV lamps. Meanwhile, the mineralization product of CO_2 is present. The reactions gradually approach a steady state after illumination for no more than 4 h. The performances of the prepared ZnO and SnO_2, the support SiO_2, and the benchmark P25 were also investigated (Figure S5-C). SiO_2 and ZnO showed no activity for the degradation of C_6H_6. After purging with the reaction gas for about 180 min, an equilibrium concentration ca. 250 ppm C_6H_6 (the exact value of the feed gas) can be reached and no CO_2 was generated even being illuminated for about 4 h (Figure S5-C-a and c). It precludes the possibility that the support (SiO_2) contributes to the degradation of C_6H_6. Although the decomposition of C_6H_6 can be realized on SnO_2 and P25, the activities are much lower than that of the prepared S-ZHS samples. What is worse, unlike S-ZHS, the color of SnO_2 and P25 turn brown (Figure 10) due to the deposition of some reaction intermediates. It suggests that the decomposition of C_6H_6 on these samples cannot sustain for a long time. In fact, as shown in Figure S5-C-d, the deactivation of SnO_2 with irradiation time can be perceived.

According to the steady-state profiles shown in Figure S5, the CE and ME of C_6H_6 on the different samples can be calculated. The results are summarized in Figure 7. It indicates that the conversion of C_6H_6 on the ZHS samples is favored by raising the solution pH, from 50.1% (pH 3) to 66% (pH 10), or the temperature, from 25.4 % (20 ^{o}C) to 66% (120 ^{o}C). By further increasing the pH to 13, the CE of ZHS-13 is only 4.1% and almost identical to the value of SnO_2. A decay of CE can be found on the sample prepared at a high temperature (150 ^{o}C). The sample prepared at 120 ^{o}C exhibits the highest CE. Although P25 shows high capability to crack BR in the degradation of MO (Figure 5l), the CE of gaseous C_6H_6 is only 9.7%. Unlike CE, the ME of C_6H_6 on the prepared S-ZHS seems less impacted (around 68%) by the solution pH, but decreases with the hydrothermal temperature, from 77.5% (20 ^{o}C) to 42.5% (150 ^{o}C). A much

higher ME of C_6H_6 is achieved on ZHS-13, SnO_2, and P25 as only minor amounts of C_6H_6 are involved in the degradation reactions. Although S-ZHS samples show lower mineralization efficiency of C_6H_6 than SnO_2 and P25, it should be noted that the efficiencies were achieved at a quite high conversion of C_6H_6 in a short contact time (1.8 s). High ME value can be expected by increasing the loading amounts of the photocatalysts or the contact time. This assumption was confirmed by a control test with 0.3 g ZHS-10 sample was loaded. The results indicated that C_6H_6 could not be detected anymore, which suggests a complete conversion of C_6H_6. Meanwhile, ca. 1200 ppm CO_2 was produced indicating a ME value of ca. 80%.

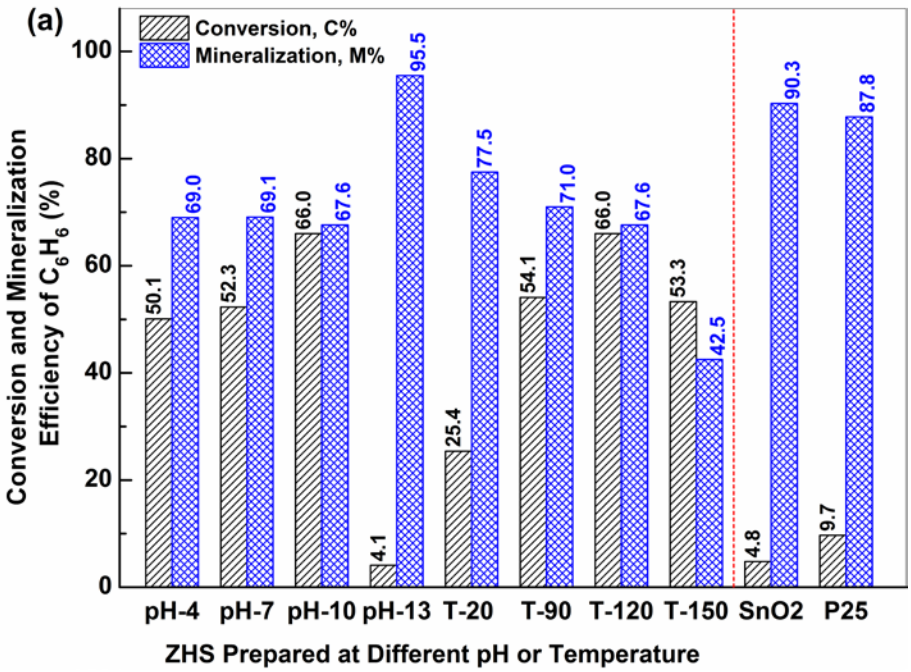

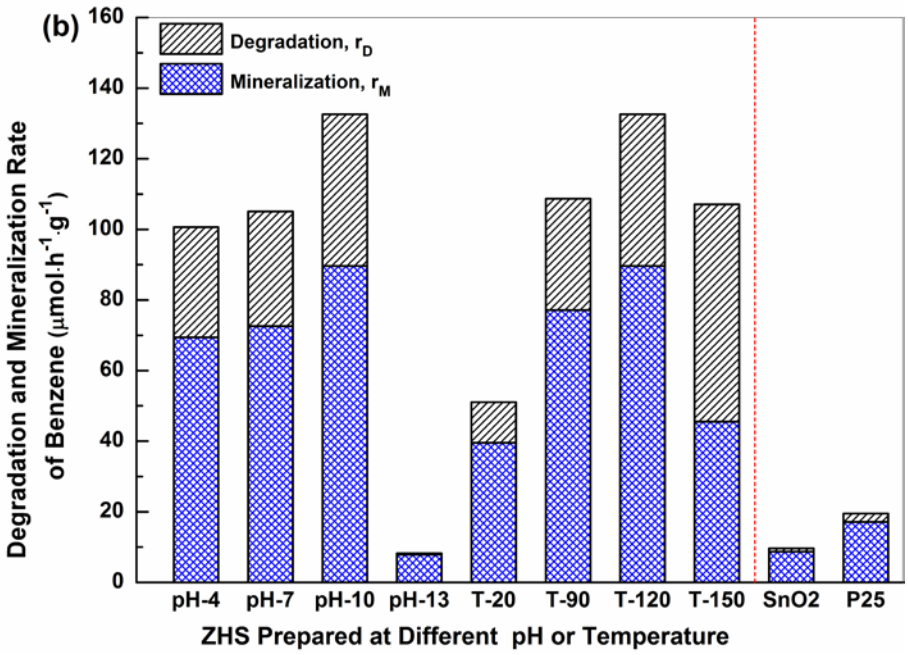

Figure 7 (a) Conversion (C%) and mineralization (M%) efficiency of C_6H_6 achieved on the prepared ZHS, SnO_2, and commercial P25; (b) Degradation (r_D) and mineralization (r_M) rates of C_6H_6 on the prepared ZHS, SnO_2, and commercial P25.

The degradation (r_D) and mineralization (r_M) rates of C_6H_6 on the photocatalysts are calculated by Eq. 3 and 4. The result is more straightforward than Figure 7a to disclose the degradation efficiency of C_6H_6 on the prepared ZHS. As shown in Figure 7b, with the change of the ZHS preparation conditions, both r_D and r_M show a same variation tendency to that of the CE shown in Figure 7a. Specifically, the rates can be improved by increasing the solution pH from 4 to 10 and then decrease sharply with further increasing the pH to 13. The improvements can also be achieved by increasing the hydrothermal temperature from 20 to 120 ^oC. However, compared to the solution pH, the enhancements are more distinct with the change of the temperature. A significant reduction of the rates is observed with further increasing the temperature to 150 ^oC, especially r_M. Apparently, the r_D and r_M of C_6H_6 obtained on the S-ZHS samples are substantially larger than that on P25, SnO_2 and the SnO_2-removed ZHS sample (i.e. ZHS-13). It

seems that the decomposition of gaseous C_6H_6 depends on both the presence of SnO_2 and ZHS components. Thus, a synergistic effect can be expected between them. The highest r_D and r_M are 132.6 and 89.6 umol·h^{-1}·g^{-1}, respectively and they are achieved on the ZHS-10. The rates are almost six times higher than that of P25. Here, we must highlight that the activity is quite remarkable because only 0.1 g photocatalyst was used and the concentration of C_6H_6 is as high as 250 ppm. More importantly, the degradation was performed in a flow mode. In most reported works, the level of C_6H_6 concentration is only several ppb or few ppm and several grams of photocatalysts were used or the degradation reaction was performed in a batch mode.[8c, 34]

3.4.3 Photocatalytic Stability of ZHS

The stability of S-ZHS was evaluated by degradation of gaseous C_6H_6 on the selected ZHS-10. The reaction was lasted for 48 h. During the reaction, the lamps were turned off intentionally for a while. The decomposition of C_6H_6 then ceases immediately as shown in Figure 8. The concentration of C_6H_6 then returns to the initial value and no CO_2 can be detected. The activity can be reactivated by switching on the lamps again. It clearly indicates that the degradation of C_6H_6 is driven by photon. No deactivation of the sample can be observed with the reaction proceeded. On contrary to the SnO_2 and P25 samples, the color of ZHS-10 is unchanged after a long-term reaction (as shown in Figure 9). XRD result (Figure S6) indicates that the crystal structure of the used sample is also not affected by the reaction.

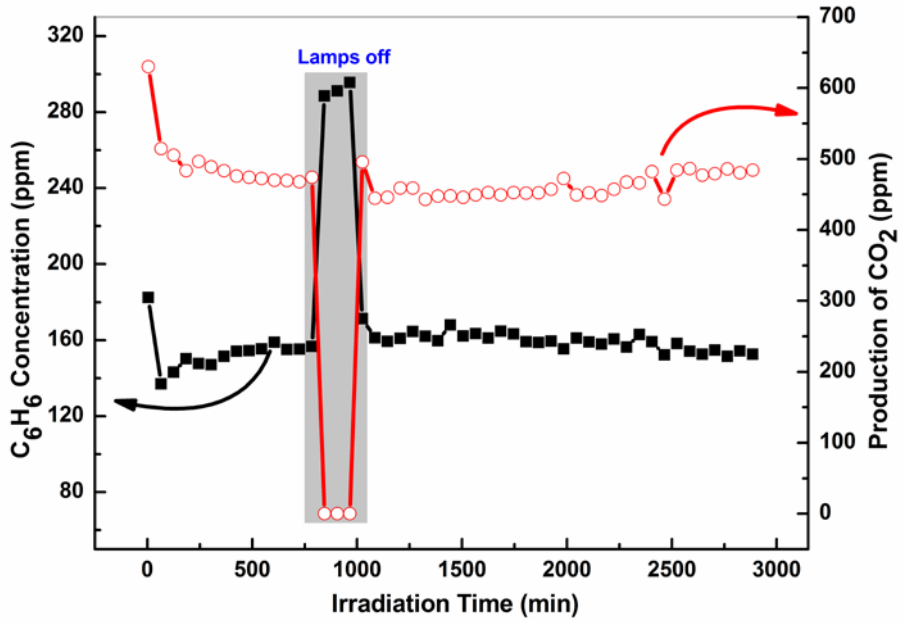

Figure 8 The long-term degradation of gaseous C_6H_6 on the ZHS-10 sample. (0.08 g sample was used).

Generally, the deactivation of a photocatalyst is mainly caused by the decomposition of itself via a photo-corrosion process, such as CdS and ZnO, or the deposition of some stable intermediates. To further confirm the stability of the ZHS-10, the depositions of the intermediates were studied by FTIR analysis. As shown in Figure 9a, the spectrum of the used sample is almost identical to the fresh one. No new absorption band can be found suggesting no stable byproduct is formed on the sample. However, as for the used SnO_2 and P25 (Figure 9b and c), some new absorption bands are present at 1482, 1400 and 1170 cm^{-1}. The band at 1480 cm^{-1} can be assigned to the C–C vibrations of the BR.[35] The other bands can be attributed to the symmetric vibration of carboxylates ($-COO^-$, 1400 cm^{-1})[33, 35a] and C-C stretching (1170 cm^{-1}) of BR[35a] or the phenolic group vibration[36]. The formation of these intermediates leads to the color change of SnO_2 and P25 from white to brown. Thus, the stability of ZHS can be largely approved by these results.

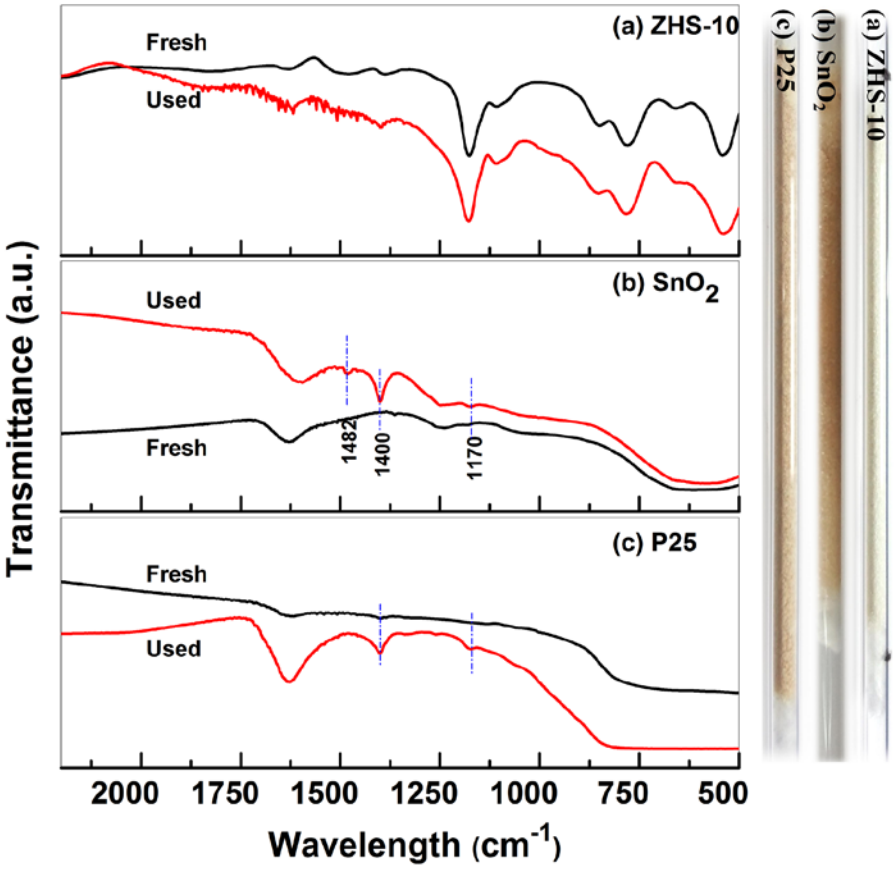

Figure 9 FTIR spectra of the samples before and after the degradation of C_6H_6: (a) sample ZHS-10, (b) SnO_2, and (c) P25. The right inset shows the digital pictures of the used samples.

3.5. Proposed Reaction Mechanism

The photocatalytic performances suggest that a synergistic effect between SnO_2 and ZHS, which accounts for the high PCO activity of the S-ZHS samples, especially for the degradation of gaseous C_6H_6. As PCO reaction is composed of a generation of active radicals and a subsequent surface degradation of C_6H_6, the synergistic effect should be understood from these two aspects. With this consideration, the active radicals formed on the ZHS-10 (as a representative of S-ZHS samples) were then determined and compared with that of the pristine SnO_2 and ZHS (i.e. ZHS-13) by ESR techniques using DMPO as a trapping reagent. The evolution of the trapped protonated $O_2^{\cdot -}$ (DMPO-·OOH, labeled with *) and ·OH (DMPO-·OH,

labeled with ♦) signals with irradiation time are shown in Figure 10A and 11B, respectively. The spectra recorded at 0 s indicate that $O_2^{\cdot-}$ and ·OH cannot be formed without irradiation. On pristine SnO_2 and $ZnSn(OH)_6$ (Figure 10A-a and b), the trapped $O_2^{\cdot-}$ signal is still hard to be perceived even after irradiation for 160 s. Their time-dependent spectra are almost identical to the corresponding background spectrum. However, the characteristic sextet peaks of the DMPO-·OOH adduct[37] can be easily identified on ZHS-10 (Figure 10A-c). As for the measurements of ·OH, with irradiation time prolonged, the characteristic quartet peaks of DMPO-·OH adduct[4a, 38] with intensity ratio ca. 1:2:2:1 can be observed on SnO_2 and ZHS-10 (Figure 10B-a and c), but hard to be distinguished on pristine $ZnSn(OH)_6$ (Figure 10B-b). Apparently, the formation of $O_2^{\cdot-}$ and ·OH on SnO_2 or ZHS-10 is induced by photons because their signals increase steadily with irradiation time. Although pristine SnO_2 and $ZnSn(OH)_6$ show low or no capability for the formation of active radicals, amazingly, a pronounced formation of $O_2^{\cdot-}$ and ·OH can be achieved on the SnO_2-decorated $ZnSn(OH)_6$, i.e. ZHS-10.

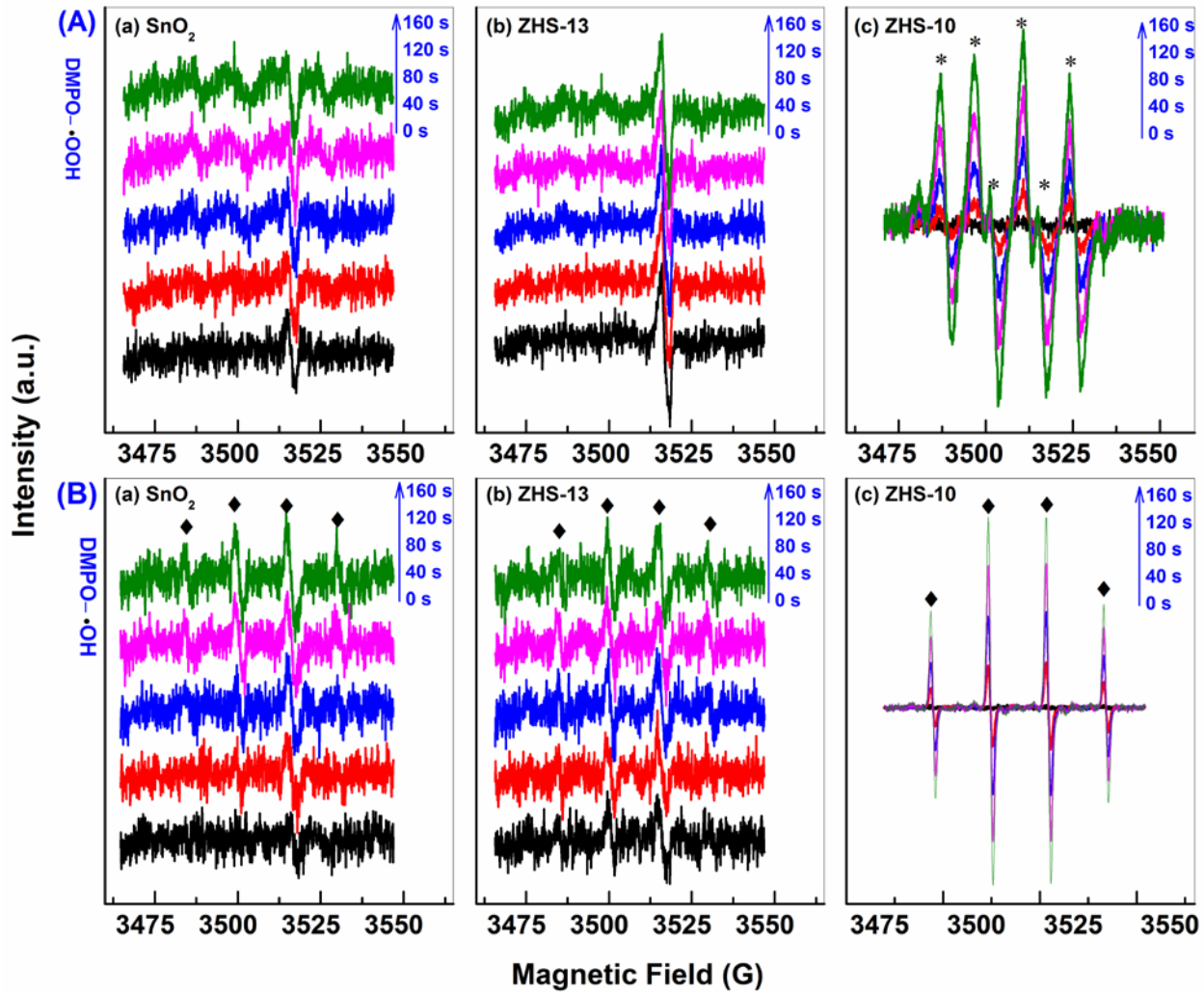

Figure 10 ESR spectra of (A) DMPO-·OOH and (B) DMPO-·OH adducts formed with irradiation time of 254 nm light in the suspension of (a) SnO_2, (b) ZHS-13, and (c) ZHS-10 samples.

The ESR results indicate that both $O_2^{\cdot-}$ and ·OH are hard to be generated on pristine $ZnSn(OH)_6$, while $O_2^{\cdot-}$ cannot be formed on SnO_2. The phenomena can be interpreted by their band structures. As shown in Figure 3, the E_g of $ZnSn(OH)_6$ is 5.0 eV, corresponding to a light wavelength of 248 nm. Therefore, $ZnSn(OH)_6$ is essentially hard to be activated by the UV lamps because the emission is mainly centered at 254 nm. This is the reason why ZHS-13 shows almost no activity for the degradation of MO and C_6H_6. As for SnO_2, although it can be

activated by the lamps, the conduction band (CB) edge of SnO_2 locates at ca. 0 V (vs. NHE)[39] and is more positive than the reduction potential of O_2 ($O_2 + e^- \rightarrow O_2{\cdot}^-$, -0.33 V vs. NHE[40]). Thus, O_2 cannot be directly reduced to $O_2{\cdot}^-$ by the photo-induced e^- in SnO_2. However, the formation of ·OH can be achieved as its valence band edge (ca. 3.5 V) is larger than the stand redox potential of ·OH/-OH (1.99 V, vs. NHE[41]). In the degradation of MO solution, since a significant activity has been observed (Figure 5k), e^- in SnO_2 is more likely to be scavenged by O_2 through a two-electro reduction process: $O_2 + 2e^- + 2H^+ \rightarrow H_2O_2$, 0.69 V vs. NHE.[40b, 42]

As $ZnSn(OH)_6$ is hard to be activated by the lamps, the pronounced formation of active radicals on ZHS-10 should be originated from SnO_2 component, which serves as a photoactive center to provide charge carriers. Thus, the role of ZHS component should be understood as a promoter for the generation of ·OH and $O_2{\cdot}^-$ rather than a photoactive center. This capability is afforded by its hydroxyl structure. ·OH is generally derived through the oxidation of surface –OH or adsorbed H_2O by h^+. The hydroxyl structure of ZHS can provide large quantities of M–OH (M=Sn or Zn) and consequently facilitates its formation. Furthermore, a sustainable formation of ·OH also can be guaranteed by the structure. In a photocatalytic process, the surface –OH will be consumed with the reaction processed (the vacancy of –OH group labeled as M^+-□). Thus the regeneration of surface –OH is an important prerequisite for a sustainable formation of ·OH. Due to its polyhydroxy surface, the adsorption of H_2O and the subsequent regeneration of –OH group can be favored by the structure. The trapping of H_2O is extremely important for the degradation of gaseous C_6H_6 as the reaction is performed in a water-deficient environment and most of the moisture comes from the degradation product of C_6H_6. Thus, an efficient and sustainable generation of ·OH can be expected on ZHS, which has been observed in our previous work.[4a]

Although O_2 cannot be directly reduced to $O_2^{\cdot -}$ on pristine SnO_2 ($O_2 + e^- \rightarrow O_2^{\cdot -}$), the formation of $O_2^{\cdot -}$ on ZHS-10 is more likely via a proton-involved reduction process $O_2 + H^+ + e^- \rightarrow HO_2^{\cdot -}$ (-0.046 V vs. NHE[42-43]) as the CB edge of SnO_2 (ca. 0 V) almost locates at the potential. The proton may come from the regeneration of –OH group: M^+-□ + H_2O →M–OH + H^+. Previous works indicated that a negative shift of the SnO_2 CB edge (from 0.06 V to -0.27 V) can be achieved by doping Zn^{2+} [44] or decoration of an insulating component like MgO[39d, 45]. In ZHS-10 sample, a similar shift of the CB edge of SnO_2 component may occur to satisfy the potential deficiency. The dopant Zn^{2+} can be provided by ZHS as some Zn^{2+} can diffuse into SnO_2[46] during the hydrothermal treatment. Here, to confirm the negative shift of the CB edge, a comparison test was performed between pure SnO_2 and Zn doped SnO_2. The samples were prepared by the similar hydrothermal methods as that of ZHS samples. As shown in Figure S7-a, both of the samples can be indexed to the tetragonal SnO_2. However, a redshift of the absorption can be observed in the Zn doped SnO_2 in Figure S7-b. Consistent with the reported work, Mott-Schottky analysis (Figure S7-c) indicate that the flat-band potential of SnO_2 moves from -0.04 to -0.11 V after doping with Zn. Besides, ZHS component may serve a similar function as that of MgO and also leads to the shift of SnO_2 CB. Although the exact reaction mechanism is still unknown, one thing is sure that $HO_2^{\cdot -}$ can be efficiently produced in the SnO_2 decorated ZHS as shown in Figure 10A-c. Furthermore, it has been demonstrated that the adsorption of O_2 is proportional to the amount of surface OH group.[7b, 47] That means the polyhydroxy structure of ZHS also favors the formation of $HO_2^{\cdot -}$.

According to the discussion, the formation processes of ·OH, $HO_2^{\cdot -}$ and the regeneration of –OH in the ZHS-10 sample are briefly described in Scheme 1.

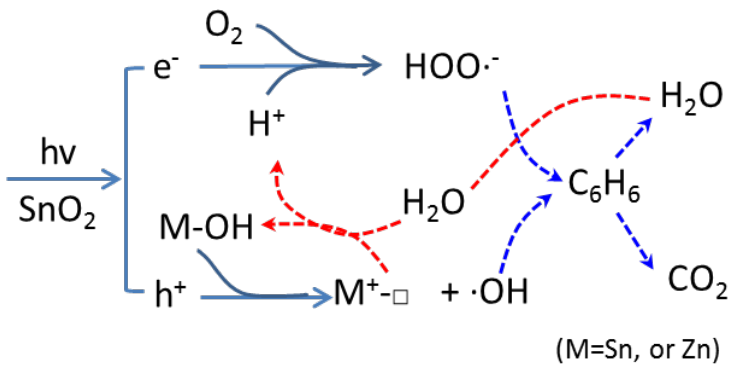

Scheme 1 Schematically describes the formation of ·OH, $HO_2\cdot^-$ and the regeneration of –OH

Besides the formation of active radicals, the degradation of C_6H_6 also benefits from ZHS. On the one hand, the opening of BR can be favored by ZHS. The degradation of MO (Figure 5k) indicates that, compared with the azo bond, the destruction efficiency of BR on SnO_2 is quite low due to the high stability of BR. However, when coupled with ZHS, the efficiency is substantially improved on the resulted S-ZHS samples. A similar improvement is also observed in the degradation of gaseous C_6H_6. It should be noted that the high activity of S-ZHS is more than a simple superposition of the performances of pristine SnO_2 and ZHS because ZHS shows almost no activity for the degradation of both MO and gaseous C_6H_6 as it is hard to be activated by the lamps. These results suggest that the opening of BR is promoted by ZHS. The role of ZHS in here should be understood as a component which can pre-activate the BR and make it vulnerable to oxidation. This capability we think is also afforded by the hydroxyl structure. Previous works[48] suggested that an OH···π electron type interaction can be formed between the surface –OH group and the aromatic ring. The enrichment of C_6H_6 on S-ZHS and the subsequent opening of BR can be favored by the interaction. On the other hand, the formation of stable intermediates in the degradation of C_6H_6, which leads to the deactivation of a photocatalyst, can be avoided by ZHS. As indicated by the ESR results, the mineralization of C_6H_6 should be induced by ·OH and $HO_2\cdot^-$. However, a h^+-mediated oxidation of C_6H_6 also can be occurred and

leads to the formation of benzene cation radicals: $C_6H_6 + h^+ \rightarrow C_6H_6^+\cdot$, 2.64 V vs NHE[49]. A polymerization of BRs then can be triggered by the cation radicals and results in a deposition of stable brown byproducts.[11c] This reaction has been observed on some oxide-type photocatalyst[3a, 11a, b]. The formation of the byproducts on pristine SnO_2 and P25 is also confirmed in this work by the change of the samples' color and the FTIR analysis (Figure 9). Consequently, with the reaction proceeded, the active sites of SnO_2 will be gradually blocked by the intractable intermediates, leading to the decay of the activity (Figure S5-C-d). However, in the presence of ZHS, h^+ is more likely captured by –OH for the high population of –OH and the lower oxidation potential to ·OH than C_6H_6 to $C_6H_6^+$ (1.99 vs. 2.64 V). Furthermore, due to the isolation of –OH group between h^+ and the adsorbed C_6H_6, the direct h^+ oxidation of C_6H_6 also can be suppressed by the adsorption behavior of C_6H_6 (OH···π interaction). Thus, ·OH mediated oxidation route can prevail over the degradation of C_6H_6 in the presence of ZHS, avoiding the h^+-induced polymerization reaction. This is the reason why no deactivation and the formation of stable intermediates are observed on ZHS-10.

In summary, the high PCO activity of S-ZHS samples for C_6H_6 degradation is the result of the synergistic effect of SnO_2 and ZHS in the formation of active radicals and the degradation of C_6H_6. The mechanism of the synergistic effect is tentatively proposed in Scheme 2. In general, SnO_2 component acts as photoactive sites to produce charge carriers which then convert to ·OH (via the process-a) and $HO_2\cdot^-$ (via the process-b, rather than to $O_2\cdot^-$ via the process-c) under UV irradiation, while ZHS component serves as preferential sites for the adsorption of the precursors including C_6H_6, O_2, and H_2O. Due to the enrichment of the reactants and the pre-activation of BR, both the formation of active radicals (process-a and b) and the degradation of benzene (process-d) can be promoted by ZHS. More importantly, the sustainability of the ·OH-dominated

oxidation of C_6H_6 can be ensured by the hydroxyl structure of ZHS, avoiding the deposition of stable byproducts induced by a direct h^+-oxidation route (process-e). Although SnO_2 amount is quite small and bare ZHS essentially shows no photocatalytic activity, both SnO_2 and ZHS are indispensable for the high activity.

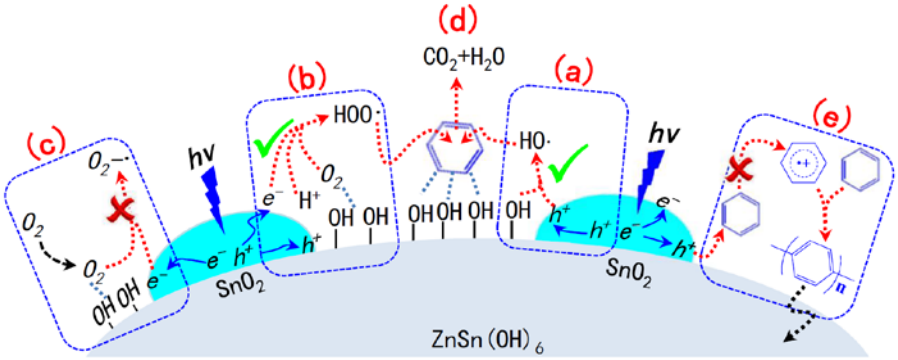

Scheme 2 Schematic representations of the mechanism of the synergistic effect between SnO_2 and ZHS in PCO of gaseous C_6H_6.

These findings provide a reliable explanation for the activity discrepancy of the reported ZHS samples[15] which were prepared in a strong alkaline solution and showed a low activity for C_6H_6 degradation. As demonstrated in this work, the poor performance of the samples should be caused by the lack of SnO_2 component which was etched by the strong alkaline solution. Because SnO_2 amount is quite small and its diffraction peaks are inconspicuous, the contribution of SnO_2 in the photocatalytic activity of ZHS has been overlooked in most of the related works.[4a, 14a, 15, 30, 50] In this work, the effect of the hydrothermal conditions on the activity of S-ZHS samples should be achieved by altering the SnO_2 amount as indicated in Figure 2 and 3. The finding also suggests that some other reported hydroxide photocatalysts, such as $In(OH)_3$, $CdSn(OH)_6$, $CaSn(OH)_6$, and $SrSn(OH)_6$,[12a, f, g] may also be contaminated by trace amount of oxides which are crucial for the high photocatalytic activity.

A novel strategy for design of high performance photocatalyst is demonstrated by this work. That is the conventional photocatalyst can be improved by coupling with some special components like the hydroxides or other insulators. These components have been seldom used for the purpose. Unlike the traditional semiconductor-semiconductor composite system, the insulation components are hard to be activated by photons and cannot serve as photocatalysts alone. However, due to their unique bulk or surface features, the capture of the reactants and the formation of the active radicals on the composites can be substantially promoted by the components. Besides ZHS, recent works indicated that h-BN,[51] Al_2O_3,[52] and MgO[53] can also play this role and the resulted composites exhibited higher photocatalytic activities than the pristine sample. The unique features of these candidates may be afforded by the hydroxyl structure or the surface electronegativity and the basicity.[51, 53a]

4. CONCLUSIONS

In summary, we synthesized a series of $ZnSn(OH)_6$ photocatalysts by a simple hydrothermal method. The effects of the treatment temperature and the solution pH on the formation and PCO activity of the samples were investigated systematically. Generally, high yield of ZHS can be achieved under a mild reaction condition (Tem. 90-120 ^{o}C, pH 4-10). However, most of the samples were contaminated by trace amount of low-crystalized SnO_2 whose formation was favored by a low treatment solution pH or a high hydrothermal temperature. Pristine ZHS can only be produced in a strong alkaline solution (pH 13) due to the etching of SnO_2. A synergistic effect between SnO_2 and ZHS has been observed in the degradation of MO solution and gaseous C_6H_6, which accounts for the high PCO performance, especially for the decomposition of C_6H_6. The sample prepared at 120 ^{o}C in a pH 10 solution shows the highest degradation rate of gaseous C_6H_6 and the efficiency is almost six times higher than P25. More importantly, no obvious

deactivation of the sample and the formation of stable deposits were observed in a long-term reaction. Although SnO_2 amount is quite small and bare ZHS essentially shows no photocatalytic activity, both SnO_2 and ZHS are indispensable for the high activity. The function of SnO_2 was proposed to be a photoactive site to produce photo-induced charge carriers, while ZHS is served as a preferential site for the adsorption of C_6H_6, O_2, and H_2O as it possesses high concentration of OH group. The pre-activation of the benzene ring and the formation of the active radicals then can be promoted by ZHS.

ASSOCIATED CONTENT

Supporting Information.

Pictures of the degradation reaction systems, the characterization (XRD, UV-Vis DRS, BET, and EIS) results of prepared samples, and the photocatalytic performance for the degradation of gaseous benzene. These materials are available free of charge via the Internet at http://pubs.acs.org.

AUTHOR INFORMATION

Corresponding Author

* (X.L. Fu) Email: fuxiliang@gmail.com

* (S. F. Chen) Email: chshifu@chnu.edu.cn

Notes

The authors declare no competing financial interest.

ACKNOWLEDGEMENTS

This work was financially supported by the Natural Science Foundation of China (Grant Nos. 21473066 and 21203029), the Natural Science Foundation of Anhui Province (Grant Nos. 1408085QB38 and 1608085QB37), the High Education Revitalization Plan of Anhui Province, and the Foundations of Natural Science of Anhui Education Committee (KJ2014A230). Prof. Shifu Chen thanks for the support of the Natural Science Foundation of China (Grant Nos. 51472005 and 51272081).

REFERENCES

(1) (a) Aksoy, M. Environ. Health Perspect. **1989**, *82*, 193-197. (b) Lan, Q.; Zhang, L.; Li, G.; Vermeulen, R.; Weinberg, R. S.; Dosemeci, M.; Rappaport, S. M.; Shen, M.; Alter, B. P.; Wu, Y.; Kopp, W.; Waidyanatha, S.; Rabkin, C.; Guo, W.; Chanock, S.; Hayes, R. B.; Linet, M.; Kim, S.; Yin, S.; Rothman, N.; Smith, M. T. Science **2004**, *306*, 1774-1776.

(2) Ren, M.; Frimmel, F. H.; Abbt-Braun, G. J. Mol. Catal. A: Chem. **2015**, *400*, 42-48.

(3) (a) Hoffmann, M. R.; Martin, S. T.; Choi, W. Y.; Bahnemann, D. W. Chemical Reviews **1995**, *95*, 69-96. (b) Mo, J.; Zhang, Y.; Xu, Q.; Lamson, J. J.; Zhao, R. *Atmos. Environ.* **2009**, *43*, 2229-2246. (c) Everaert, K.; Baeyens, J. J. Hazard. Mater. **2004**, *109*, 113-139. (d) Chiang, Y.-C.; Chiang, P.-C.; Huang, C.-P. Carbon **2001**, *39*, 523-534.

(4) (a) Fu, X.; Wang, X.; Ding, Z.; Leung, D. Y. C.; Zhang, Z.; Long, J.; Zhang, W.; Li, Z.; Fu, X. *Appl. Catal., B* **2009**, *91*, 67-72. (b) Kim, S. B.; Hwang, H. T.; Hong, S. C. *Chemosphere* **2002**, *48*, 437-444. (c) Einaga, H.; Futamura, S.; Ibusuki, T. *Phys. Chem. Chem. Phys*. **1999**, *1*, 4903-4908. (d) Huang, J.; Wang, X.; Hou, Y.; Chen, X.; Wu, L.; Fu, X. *Environ. Sci. Technol.* **2008**, *42*, 7387-7391.

(5) (a) Du, J.; Chen, W.; Zhang, C.; Liu, Y.; Zhao, C.; Dai, Y. *Chem. Eng. J.* **2011**, *170*, 53-58. (b) He, F.; Li, J.; Li, T.; Li, G. *Chem. Eng. J.* **2014**, *237*, 312-321.

(6) (a) Belver, C.; López-Muñoz, M. J.; Coronado, J. M.; Soria, *J. Appl. Catal., B* **2003**, *46*, 497-509. (b) Einaga, H.; Ibusuki, T.; Futamura, S. *Environ. Sci. Technol.* **2004**, *38*, 285-289.

(7) (a) Fu, X.; Zeltner, W. A.; Anderson, M. A. *Appl. Catal., B* **1995**, *6*, 209-224. (b) Ibusuki, T.; Takeuchi, K. *Atmos. Environ.* **1986**, *20***,** 1711-1715. (c) Chen, Y.; Li, D.; Wang, X.; Wang, X.; Fu, X. *Chem. Commun.* **2004**, *10*, 2304-2305.

(8) (a) Huang, H.; Li, D.; Lin, Q.; Zhang, W.; Shao, Y.; Chen, Y.; Sun, M.; Fu, X. *Environ. Sci. Technol.* **2009**, *43*, 4164-4168. (b) Xue, H.; Li, Z.; Wu, L.; Ding, Z.; Wang, X.; Fu, X. *J. Phys. Chem. C* **2008**, *112*, 5850-5855. (c) Zeng, M.; Li, Y.; Mao, M.; Bai, J.; Ren, L.; Zhao, X. *ACS Catal.* **2015**, 3278-3286.

(9) (a) Pelizzetti, E.; Minero, C. *Electrochim. Acta* **1993**, *38*, 47-55. (b) Du, P.; Bueno-López, A.; Verbaas, M.; Almeida, A. R.; Makkee, M.; Moulijn, J. A.; Mul, G. *J. Catal.* **2008**, *260*, 75-80.

(10) (a) Shafaei, A.; Nikazar, M.; Arami, M. *Desalination* **2010**, *252*, 8-16. (b) Tran, H.; Chiang, K.; Scott, J.; Amal, R. *Photochem. Photobiol. Sci.* **2005**, *4*, 565-567.

(11) (a) D' Hennezel, O.; Pichat, P.; Ollis, D. F. *J. Photochem. Photobiol.*, A **1998**, *118*, 197-204. (b) Sitkiewitz, S.; Heller, *A. New J. Chem.* **1996**, *20***,** 233-241. (c) Yamamoto, K.; Asada, T.; Nishide, H.; Tsuchida, E. Bull. *Chem. Soc. Jpn.* **1988**, *61*, 1731-1734.

(12) (a) Meng, S.; Li, D.; Sun, M.; Li, W.; Wang, J.; Chen, J.; Fu, X.; Xiao, G. *Catal. Commun.* **2011**, *12*, 972-975. (b) Yan, T.; Long, J.; Shi, X.; Wang, D.; Li, Z.; Wang, X. *Environ. Sci. Technol.* **2010**, *44*, 1380-1385. (c) Sun, M.; Li, D. Z.; Chen, Y. B.; Chen, W.; Li, W. J.; He, Y. H.; Fu, X. Z. *J. Phys. Chem. C* **2009**, *113*, 13825-13831. (d) Sun, M.; Li, D.; Zhang, W.; Fu, X.; Shao, Y.; Li, W.; Xiao, G.; He, Y. *Nanotechnol.* **2010**, *21*, 355601. (e) Li, Z. H.; Xie, Z. P.; Zhang, Y. F.; Wu, L.; Wang, X. X.; Fu, X. Z. *J. Phys. Chem. C* **2007**, *111*, 18348-18352. (f) Yan, T.; Wang, X.; Long, J.; Liu, P.; Fu, X.; Zhang, G.; Fu, X. *J. Colloid*

Interface Sci. **2008**, *325*, 425-431. (g) Luo, Y.; Chen, J.; Liu, J.; Shao, Y.; Li, X.; Li, D. *Appl. Catal., B* **2016**, *182*, 533-540.

(13) Fu, X.; Leung, D. Y. C.; Wang, X.; Xue, W.; Fu, X. *Int. J. Hydrogen Energy* **2011**, *36*, 1524-1530.

(14) (a) Chen, Y.; Li, D.; He, M.; Hu, Y.; Ruan, H.; Lin, Y.; Hu, J.; Zheng, Y.; Shao, Y. *Appl. Catal., B* **2012**, *113–114*, 134-140. (b) Wang, M.; Cao, X.; Huang, Y.; Guo, C.; Huang, L.; Yin, S.; Sato, T. *CrystEngComm* **2012**, *14*, 2950-2953. (c) Wang, L.; Tang, K.; Liu, Z.; Wang, D.; Sheng, J.; Cheng, W. *J. Mater. Chem.* **2011**, *21*, 4352-4357.

(15) (a) Yu, H.; Lai, R.; Zhuang, H.; Zhang, Z.; Wang, X. *CrystEngComm* **2012**, *14*, 8530-8535. (b) Fu, X.; Huang, D.; Qin, Y.; Li, L.; Jiang, X.; Chen, S. *Appl. Catal., B* **2014**, *148-149*, 532-542.

(16) Zeng, J.; Xin, M. D.; Li, K. W.; Wang, H.; Yan, H.; Zhang, W. J. *J. Phys. Chem. C* **2008**, *112*, 4159-4167.

(17) Xu, X.; Duan, G.; Li, Y.; Zhang, H.; Liu, G.; Cai, W. *CrystEngComm* **2013**, *15*, 6159-6164.

(18) (a) Choi, W. K.; Sung, H.; Kim, K. H.; Cho, J. S.; Choi, S. C.; Jung, H. J.; Koh, S. K.; Lee, C. M.; Jeong, K. *J. Mater. Sci. Lett.* **1997**, *16*, 1551-1554. (b) He, Y.; Li, D.; Chen, J.; Shao, Y.; Xian, J.; Zheng, X.; Wang, P. *RSC Adv.* **2014**, *4*, 1266-1269.

(19) (a) Xia, W.; Wang, H.; Zeng, X.; Han, J.; Zhu, J.; Zhou, M.; Wu, S. *Crystengcomm* **2014**, *16*, 6841-6847. (b) Mäki-Jaskari, M. A.; Rantala, T. T. *Model. Simul. Mater. Sci. Eng.* **2004**, *12*, 33-41.

(20) Mathur, S.; Ganesan, R.; Grobelsek, I.; Shen, H.; Ruegamer, T.; Barth, S. *Adv. Eng. Mater.* **2007**, *9*, 658-663.

(21) (a) Arai, T.; Adachi, S. *ECS J Solid State Sci. Technol.* **2012**, *1*, R15-R21. (b) Arai, T.; Adachi, S. *Jap. J Appl. Phys.* **2012**, *51*, 105002.

(22) Wang, Z.; Wang, Z.; Wu, H.; Lou, X. W. *Sci. rep.* **2013**, *3*, 1391.

(23) Brückner, A. *Catal. Rev.* **2003**, *45*, 97-150.

(24) (a) Shah, P.; Ramaswamy, A. V.; Lazar, K.; Ramaswamy, V. *Microporous Mesoporous Mater.* **2007**, *100*, 210-226. (b) Seftel, E. M.; Popovici, E.; Mertens, M.; Stefaniak, E. A.; Van Grieken, R.; Cool, P.; Vansant, E. F. *Appl. Catal., B* **2008**, *84*, 699-705. (c) Seftel, E. M.; Puscasu, M. C.; Mertens, M.; Cool, P.; Carja, G. *Appl. Catal., B* **2015**, *164*, 251-260.

(25) (a) Ge, S.; Zhang, L. *Environ. Sci. Technol.* **2011**, *45*, 3027-3033. (b) Liu, C.; Chen, H.; Ren, Z.; Dardona, S.; Piech, M.; Gao, H.; Gao, P.-X. *Appl. Surf. Sci.* **2014**, *296*, 53-60.

(26) Tauc, J.; Grigorovici, R.; Vancu, A. *physica status solidi (b)* **1966**, *15*, 627-637.

(27) Sinha, A. K.; Pradhan, M.; Sarkar, S.; Pal, T. *Environ. Sci. Technol.* **2013**, *47*, 2339-2345.

(28) Chen, G.; Ji, S.; Sang, Y.; Chang, S.; Wang, Y.; Hao, P.; Claverie, J.; Liu, H.; Yu, G. *Nanoscale* **2015**, *7*, 3117-3125.

(29) Yin, J.; Gao, F.; Wei, C.; Lu, Q. *Inorg. Chem.* **2012**, *51*, 10990-10995.

(30) Tian, Z. F.; Liang, C. H.; Liu, J.; Zhang, H. M.; Zhang, L. D. *J. Mater. Chem.* **2012**, *22*, 17210-17214.

(31) Fan, C. M.; Peng, Y.; Zhu, Q.; Lin, L.; Wang, R. X.; Xu, A. W. *J. Phys. Chem. C* **2013**, *117*, 24157-24166.

(32) Tasaki, T.; Wada, T.; Fujimoto, K.; Kai, S.; Ohe, K.; Oshima, T.; Baba, Y.; Kukizaki, M. *J. Hazard. Mater.* **2009**, *162*, 1103-1110.

(33) Cao, L.; Gao, Z.; Suib, S. L.; Obee, T. N.; Hay, S. O.; Freihaut, J. D. *J. Catal.* **2000**, *196*, 253-261.

(34) (a) Liu, Y.; Shu, W.; Chen, K.; Peng, Z.; Chen, W. *ACS Catal.* **2012**, *2*, 2557-2565. (b) Strini, A.; Cassese, S.; Schiavi, L. *Appl. Catal., B* **2005**, *61*, 90-97. (c) Jo, W. K.; Park, J. H.; Chun, H. D. *J. Photochem. Photobiol.*, A **2002**, *148*, 109-119. (d) Jo, W. K.; Park, K. H. *Chemosphere* **2004**, *57*, 555-565.

(35) (a) Wu, W.-C.; Liao, L.-F.; Lien, C.-F.; Lin, J.-L. *Phys. Chem. Chem. Phys*. **2001**, *3*, 4456-4461. (b) Zhuang, H.; Gu, Q.; Long, J.; Lin, H.; Lin, H.; Wang, X. *RSC Adv.* **2014**, *4*, 34315-34324.

(36) Volkamer, R.; Klotz, B.; Barnes, I.; Imamura, T.; Wirtz, K.; Washida, N.; Becker, K. H.; Platt, U. *Phys. Chem. Chem. Phys*. **2002**, *4*, 1598-1610.

(37) (a) Brezova, V.; Tarabek, P.; Dvoranova, D.; Stasko, A.; Biskupic, S. *J Photoch Photobio A* **2003**, *155*, 179-**198.** (b) Chen, F.; Xie, Y.; He, J.; Zhao, J. *J. Photochem. Photobiol.*, A **2001**, *138*, 139-146. (c) Chen, C.; Ma, W.; Zhao, *J. Chem. Soc. Rev.* **2010**, *39*, 4206-4219.

(38) Li, Y.; Wen, B.; Yu, C.; Chen, C.; Ji, H.; Ma, W.; Zhao, *J. Chem. Eur. J.* **2012**, *18*, 2030-2039.

(39) (a) Kawahara, T.; Doushita, K.; Tada, H. *J. Sol-Gel Sci. Technol.* **2003**, *27*, 301-307. (b) Siedl, N.; Baumann, S. O.; Elser, M. J.; Diwald, O. *J. Phys. Chem. C* **2012**, *116*, 22967-22973. (c) Lin, X. P.; Huang, F. Q.; Xing, J. C.; Wang, W. D.; Xu, F. F. *Acta Mater.* **2008**, *56*, 2699-2705. (d) Bandara, J.; Ranasinghe, R. A. S. S. *Appl. Catal. A* **2007**, *319*, 58-63.

(40) (a) Chai, Y.; Ding, J.; Wang, L.; Liu, Q.; Ren, J.; Dai, W. L. *Appl. Catal., B* **2015**, *179*, 29-36. (b) Kim, J.; Lee, C. W.; Choi, W. *Environ. Sci. Technol.* **2010**, *44*, 6849-6854.

(41) (a) Li, K.; Gao, S.; Wang, Q.; Xu, H.; Wang, Z.; Huang, B.; Dai, Y.; Lu, J. *ACS Appl. Mater. Interfaces* **2015**, *7*, 9023-9030. (b) Huang, J.; Ho, W.; Wang, X. *Chem. Commun.* **2014**, *50*, 4338-4340.

(42) Wang, C.; Zhang, X.; Liu, Y. *Appl. Surf. Sci.* **2015**, 10.1016/j.apsusc.**2015**.08.055.

(43) Ouyang, S.; Ye, J. *J. Am. Chem. Soc.* **2011**, *133*, 7757-7763.

(44) Li, Z.; Zhou, Y.; Yu, T.; Liu, J.; Zou, Z. *CrystEngComm* **2012**, *14*, 6462-6468.

(45) Bandara, J.; Pradeep, U. W. *Thin Solid Films* **2008**, *517*, 952-956.

(46) Zheng, L.; Zheng, Y.; Chen, C.; Zhan, Y.; Lin, X.; Zheng, Q.; Wei, K.; Zhu, J. *Inorg. Chem*. **2009**, *48*, 1819-1825.

(47) Henderson, M. A.; Epling, W. S.; Peden, C. H. F.; Perkins, C. L. *J. Phys. Chem. B* **2002**, *107*, 534-545.

(48) (a) Nagao, M.; Suda, Y. *Langmuir* **1989**, *5*, 42-47. (b) Lin, H.; Long, J.; Gu, Q.; Zhang, W.; Ruan, R.; Li, Z.; Wang, X. *Phys. Chem. Chem. Phys*. **2012**, *14*, 9468-9474.

(49) (a) Merkel, P. B.; Luo, P.; Dinnocenzo, J. P.; Farid, S. *J. Org. Chem.* **2009**, *74*, 5163-5173. (b) Ohkubo, K.; Fujimoto, A.; Fukuzumi, S. *J. Am. Chem. Soc.* **2013**, *135*, 5368-5371.

(50) Lopes, O. F.; de Mendonca, V. R.; Umar, A.; Chuahan, M. S.; Kumar, R.; Chauhan, S.; Ribeiro, C. *New J. Chem.* **2015**, *39*, 4624-4630.

(51) Fu, X.; Hu, Y.; Yang, Y.; Liu, W.; Chen, S. *J. Hazard. Mater.* **2013**, *244–245*, 102-110.

(52) (a) Fu, X.; Tang, W.; Ji, L.; Chen, S. *Chem. Eng. J.* **2012**, *180*, 170-177. (b) Le Formal, F.; Tétreault, N.; Cornuz, M.; Moehl, T.; Grätzel, M.; Sivula, K. *Chem. Sci.* **2011**, *2*, 737-743.

(53) (a) Xie, S. J.; Wang, Y.; Zhang, Q. H.; Fan, W. Q.; Deng, W. P.; Wang, Y. *Chem. Commun.* **2013**, *49*, 2451-2453. (b) Chen, S.; Shen, S.; Liu, G.; Qi, Y.; Zhang, F.; Li, C. *Angew. Chem. Int. Ed.* **2015**, *54*, 3047-3051.

Table of Contents Graphic and Synopsis